ORGANOMETALLICS

pubs.acs.org/Organometallics Article

Bimetallic Co−M (M = Cu, Ag, and Au) Carbonyl Complexes Supported by *N*-Heterocyclic Carbene Ligands: Synthesis, Structures, Computational Investigation, and Catalysis for Ammonia Borane Dehydrogenation

Cristiana Cesari, Beatrice Berti, Francesco Calcagno, Carlo Lucarelli, Marco Garavelli, Rita Mazzoni, Ivan Rivalta, and Stefano Zacchini*

Cite This: *Organometallics* 2021, 40, 2724−2735 Read Online

ACCESS | Metrics & More | Article Recommendations | Supporting Information

ABSTRACT: The reaction of $Na[Co(CO)_4]$ with M(IPr)Cl (M = Cu, Ag, and Au; IPr = $C_3N_2H_2(C_6H_3{}^iPr_2)_2$) affords the neutral heterometallic complexes $[Co(CO)_4\{M(IPr)\}]$ (M = Cu, **1**; Ag, **2**; and Au, **3**). Formation of **2** is accompanied by traces of $[Ag(IPr)_2][Ag\{Co(CO)_4\}_2]$ (**4**). The reaction of $Na[Co(CO)_4]$ with M(IMes)Cl (IMes = $C_3N_2H_2(C_6H_2Me_3)_2$) results in mixtures of $[Co(CO)_4\{M(IMes)\}]$ (M = Cu, **5**; Ag, **6**; and Au, **7**) and $[M(IMes)_2][M\{Co(CO)_4\}_2]$ (M = Cu, **8**; Ag, **9**; and Au, **10**). In the cases of Cu and Ag, ionic complexes **8** and **9** are the major products, whereas neutral species **7** is the major product for Au. All species **1**−**10** have been spectroscopically characterized by IR and ^1H and $^{13}C\{^1H\}$ NMR spectroscopy. Moreover, the molecular structures of **2**, **3**, and **8** have been determined by single-crystal X-ray diffraction (SC-XRD). Bimetallic Co−M−NHC complexes **1**−**3** and **7**−**9** have been tested as catalysts for the dehydrogenation of ammonia−borane (AB) in THF as solvent, and their performances compared to $[Fe(CO)_4\{M(NHC)\}_2]$, M(NHC)Cl, and $Na[Co(CO)_4]$. DFT computations have been performed to provide information on the structure, IR spectroscopy, and the thermodynamics of Co−M carbonyl clusters.

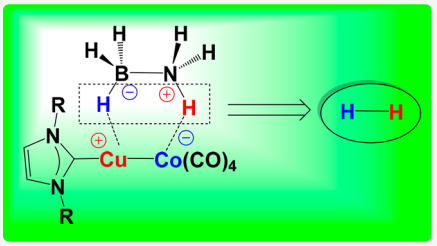

1. INTRODUCTION

Heterometallic complexes and clusters represent an emerging class of compounds for the activation of small molecules and catalytic applications.[1−4] Heterobimetallic catalysts of the type (NHC)M−$[M'_{CO}]$ (NHC = *N*-heterocyclic carbene; M = Cu, Ag, and Au, and ZnCl; $[M'_{CO}]$ = $FeCp(CO)_2$, $Mn(CO)_5$, $WCp(CO)_3$, and $Co(CO)_4$) can be assembled upon mixing M(NHC)Cl and $[M'_{CO}]^-$ precursors.[1,5] Because of the polarization of the M−M′ bond of (NHC)M−$[M'_{CO}]$, M is positively charged (electrophilic character), and M′ is negatively charged (nucleophilic character). Activation of small molecules (e.g., H_2, CS_2, and N_2O) is obtained under mild conditions due to this cooperative bifunctionality. Heterometallic systems containing a coinage metal and a metal carbonyl fragment may be described as metal-only Lewis pairs, since they contain a transition metal Lewis acid (coinage metal) and a transition metal Lewis base (metal carbonyl fragment). In this respect, they resemble main group frustrated Lewis pairs (FLPs).[4,6−8]

Several heterometallic complexes of the type $[Fe(CO)_4\{M(NHC)\}]^-$, $[Fe(CO)_4\{M(NHC)\}_2]$, and $[Fe(CO)_4\{Zn(IPr)\}]_2$ (M = Cu, Ag, and Au; NHC = $C_3N_2H_2(C_6H_2Me_3)_2$ (IMes) and $C_3N_2H_2(C_6H_3{}^iPr_2)_2$ (IPr)) can be prepared starting from the Collman reagent $Na_2Fe(CO)_4$.[5,9−13] $[Fe(CO)_4\{Cu(IPr)\}_2]$ displays bifunctional N_2O activation and is a promising candidate for CO_2 and other small-molecule activation.[5] In contrast, the chemistry of related $[Co(CO)_4]^-$-based systems is less developed, and to the best of our knowledge, only the compounds $[Co(CO)_4\{Cu(IPr)\}]$ and $[Cu(IMes)_2][Cu\{Co(CO)_4\}_2]$ have been previously described.[1]

Ammmonia−borane (NH_3BH_3, AB) dehydrogenation may represent a proof-of-concept target for bifunctional activation by means of heterometallic complexes. Indeed, AB contains both hydridic (B−H) and protic (N−H) hydrogens, which could be activated by interaction with the Lewis acid site and the Lewis base site, respectively, of a heterometallic metal-only Lewis pair.[14] AB dehydrogenation is a very interesting reaction for the potential application of AB as hydrogen storage medium for transportation.[15−20] Several monometallic transition metal complexes have been investigated as catalysts for AB dehydrogenation, including NHC complexes and the use of noninnocent ligands and homometallic carbonyls.[21−24] Bifunctional AB dehydrogenation may be promoted by $[L_nM]$−H transition metal hydrides,[25] where the $[L_nM]$ fragment acts as

Received: June 17, 2021
Published: July 30, 2021

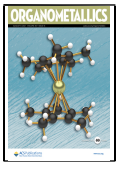

Scheme 1. Syntheses of the Complexes

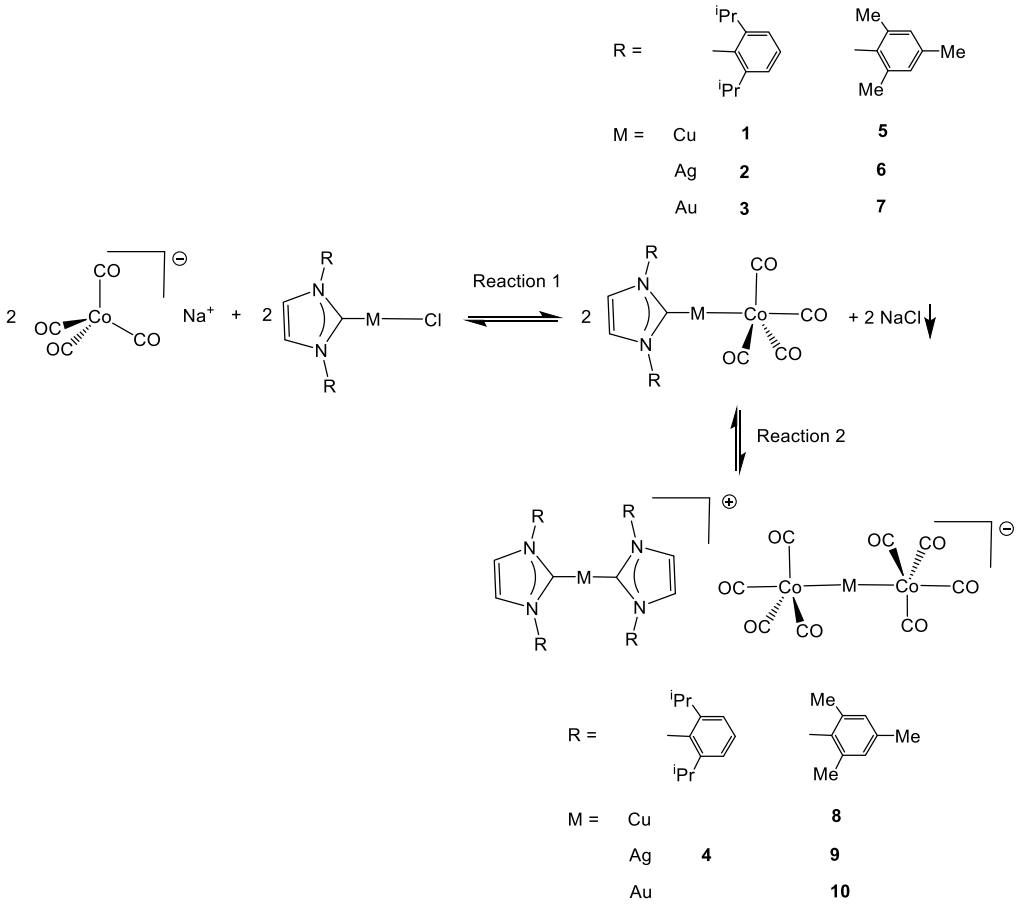

Lewis acid and the hydride holds a negative charge (Lewis base). Thus, it was of interest to test heterometallic complexes containing both acid and base metal sites for the same reaction.

Herein, we report a detailed study on the reactions of $Na[Co(CO)_4]$ with M(NHC)Cl (M = Cu, Ag, and Au; NHC = IMes and IPr), which results in heterometallic Co−M complexes. These have been characterized in solution by means of spectroscopic methods (IR and NMR), and their molecular structures are revealed by single-crystal X-ray diffraction (SC-XRD). The new heterometallic complexes have been tested as catalysts for AB dehydrogenation, and their behavior in solution was further elucidated by means of DFT methods.

2. RESULTS AND DISCUSSION

2.1. Synthesis and Characterization. The reactions of $Na[Co(CO)_4]$ with M(NHC)Cl (M = Cu, Ag, and Au; NHC = IMes and IPr) have been carried out by mixing the two species in THF in equimolar amounts and stirring at room temperature for 1 h. The outcome of the reactions depends on the nature of M and NHC. The general synthesis scheme involves two reactions as depicted in Scheme 1. Precipitation of NaCl seems to be the driving force of the first reaction. Thus, by using $[PPN][Co(CO)_4]$ ($[PPN]^+ = [N(PPh_3)_2]^+$) instead of $Na[Co(CO)_4]$, no reaction was observed. Moreover, reaction (1) is favored by low polarity solvents such as CH_2Cl_2 and THF, whereas more polar solvents such as CH_3CN and dmso lead to dissociation of the Co−M adducts and formation of the starting $[Co(CO)_4]^-$ anion. Reaction (2) involves the self-ionization of $[Co(CO)_4\{M(NHC)\}]$ to $[M(NHC)_2]^+$ and $[M\{Co(CO)_4\}_2]^-$. This second reaction is strongly influenced by the nature of NHC and M.

When NHC = IPr, the neutral complexes $[Co(CO)_4\{M(IPr)\}]$ (M = Cu, **1**; Ag, **2**; and Au, **3**) are the major species obtained as evidenced by IR spectroscopy (Figures S1−S6). Indeed, for M = Cu and Au, **1** and **3** are the only species formed, whereas there is no evidence for ionic compounds such as $[Cu(IPr)_2][Cu\{Co(CO)_4\}_2]$ and $[Au(IPr)_2][Au\{Co(CO)_4\}_2]$. Thus, **1** displays ν_{CO} bands in CH_2Cl_2 solution at 2041 (s), 1960 (s), 1935 (s), and 1913 (sh) cm^{-1} as previously reported in the literature.[1] In more polar solvents such as CH_3CN and dmso, the intensities of these bands decrease and a strong band at 1889 cm^{-1} typical of $[Co(CO)_4]^-$ appears. This indicates that according to reaction (1) in polar solvents **1** dissociates into $[Co(CO)_4]^-$ and $[Cu(IPr)(solv)]^+$. Similarly, **3** displays ν_{CO} bands in CH_2Cl_2 solution at 2047 (s), 1968 (s), and 1951 (s) cm^{-1}, and dissociation is observed in more polar solvents, even if to a lower extent compared to that of **1**. The nature of **3** has been further corroborated by means of SC-XRD (Figure 1) and ^1H and $^{13}C\{^1H\}$ NMR analyses (Figures S9 and S10).

The reaction between $Na[Co(CO)_4]$ and Ag(IPr)Cl is slightly more complicated, since it affords **2** as the major product, accompanied by traces of $[Ag(IPr)_2][Ag\{Co(CO)_4\}_2]$ (**4**) and $[Co(CO)_4]^-$, as clearly evidenced by IR spectroscopy (Figure S2). After workup, **2** has been isolated, and its molecular structure determined by SC-XRD (Figure 2). Complex **2** seems to be in equilibrium with **4**, as evidenced by IR spectroscopy. Indeed, the ν_{CO} bands of **4**, even if

https://doi.org/10.1021/acs.organomet.1c00363
Organometallics 2021, 40, 2724−2735

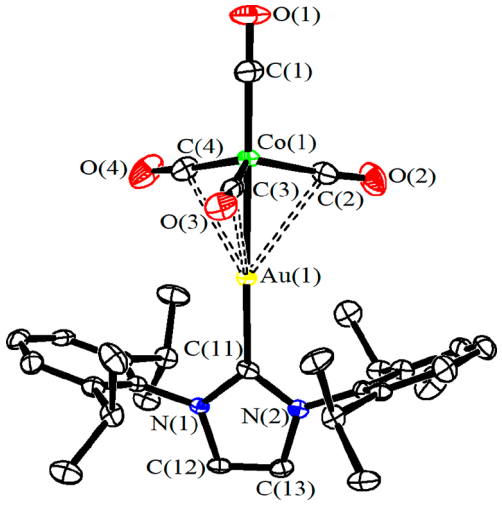

Figure 1. Molecular structure of $[Co(CO)_4\{Au(IPr)\}]$ (**3**). Thermal ellipsoids are at the 50% probability level. Au···C(O) contacts [2.67−2.86 Å] are represented as fragmented lines. Hydrogen atoms have been omitted for clarity (green, Co; yellow, Au; blue, N; red, O; gray, C). Main bond distances (Å) and angles (deg): Co−Au 2.5132(5), Au−$C_{carbene}$ 2.007(4), Co−C(O) 1.775(5)-1.781(4), Co−Au−$C_{carbene}$ 178.21(12).

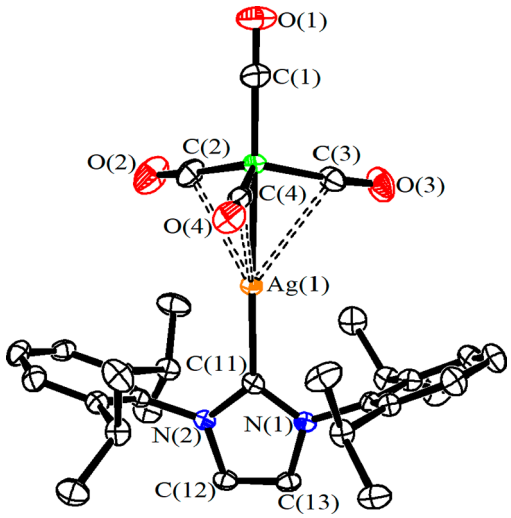

Figure 2. Molecular structure of $[Co(CO)_4\{Ag(IPr)\}]$ (**2**). Thermal ellipsoids are at the 50% probability level. Ag···C(O) contacts [2.71−2.85 Å] are represented as fragmented lines. Hydrogen atoms have been omitted for clarity (green, Co; orange, Ag; blue, N; red, O; gray, C). Main bond distances (Å) and angles (deg): Co−Ag 2.5344(3), Ag−$C_{carbene}$ 2.1062(19), Co−C(O) 1.774(3)−1.781(2), Co−Ag−$C_{carbene}$ 177.49(6).

significantly weaker, are also always present in solution by dissolving the pure crystals of **2**. Moreover, by employing polar solvents such as CH_3CN and dmso, the ν_{CO} band of $[Co(CO)_4]^-$ is also present beside those of **2** and **4**.

The molecular structures of **2** and **3** are very similar to that previously reported for **1**,[1] as well as $[Co(CO)_4\{Au(PPh_3)\}]$[26] and the monoanions $[Fe(CO)_4\{M(IPr)\}]^-$ (M = Cu and Au) and $[Fe(CO)_4\{Au(IMes)\}]^-$.[9,11] Complexes **1**−**3** adopt a trigonal bipyramidal (TBP) structure, with the M(NHC) fragment in an axial position. They contain close M−Co, Co−C(O), and M−$C_{carbene}$ interactions as well as some weak M···C(O) contacts. The nature of the latter contacts is rather debated in the literature, since they could be merely due to steric requirements of the CO ligands, rather than any real attraction (even van der Waals) between the carbonyls and the coinage metal.[27] M···C(O) contacts in Figures 1−4 have been represented as dotted lines for distances below the sum of the van der Waal radii of C and M. Such contacts are further discussed in section 2.3.

The Co−M distances of **1**−**3** can be compared using Cotton's formal shortness ratio (FSR),[28] which accounts for the different metal sizes on the basis of the differences of their Pauling's atomic radii (Co 1.157 Å, Cu 1.173 Å, Ag 1.339 Å, and Au 1.336 Å).[29] The FSR values for **1**−**3** (Table 1) are very close to 1, as expected for single bonds. Actually, the FSR value of **2** (1.015) is slightly greater than those of **1** (1.005) and **3** (1.008), suggesting a slight elongation of the Co−Ag bond compared to Co−Cu and Co−Au, even if the difference is very small. Moreover, the Co−Au distance of **3** [2.5132(5) Å, FSR 1.008] is very similar to that found in $[Co(CO)_4\{Au(PPh_3)\}]$ [2.503 Å, FSR 1.004].[26]

Table 1. Co−M Distances (Å) and Formal Shortness Ratio (FSR) of 1−3

complex	Co−M (Å)	FSR
1[a]	2.3423(6)	1.005
2	2.5344(3)	1.015
3	2.5132(5)	1.008

[a]From ref 1.

Compounds **1**−**3** have been also characterized by means of ^1H and $^{13}C\{^1H\}$ NMR spectroscopy (Figures S7−S14). Data for **1** are in accord to the literature. The CO ligands of **2** and **3** show a broad resonance at 205.8 and 207.6 ppm, respectively, in the $^{13}C\{^1H\}$ NMR spectrum, in view of the high quadrupole moment of cobalt. This broadening is probably the reason why the carbonyl resonance was not observed in the case of **1**.[1] The carbene carbon appears as a singlet at δ_C 187.2 ppm in the $^{13}C\{^1H\}$ NMR spectrum of **3**, whereas two doublets with $^1J_{C-109Ag}$ = 234 and $^1J_{C-107Ag}$ = 202 Hz centered at δ_C 185.3 ppm are present in the case of **2**.

When NHC = IMes, both neutral species $[Co(CO)_4\{M(IMes)\}]$ (M = Cu, **5**; Ag, **6**; and Au, **7**) and ionic complexes $[M(IMes)_2][M\{Co(CO)_4\}_2]$ (M = Cu, **8**; Ag, **9**; and Au, **10**) are formed in mixture, even if their relative ratio strongly depends of M. Thus, in the case of Cu and Ag, ionic species **8** and **9** are the major products observed by IR spectroscopy, and only traces of **5** and **6** are detected. In contrast, in the case of Au, neutral species **7** is the major product formed, whereas only traces of ionic compound **10** have been detected. Indeed, the IR spectra in solution of all these species show two strong and broader ν_{CO} bands in the region of 1930−1968 cm^{-1}, as well as a sharper band at 2022−2026 cm^{-1} for the ionic species $[M(NHC)_2][M\{Co(CO)_4\}_2]$, that moves to 2038−2047 cm^{-1} for the neutral species $[Co(CO)_4\{M(NHC)\}]$ (Figures S5 and S6).

The molecular structure of **9** has been also confirmed by SC-XRD. It consists of an ionic packing of $[Ag(IMes)_2]^+$ cations and $[Ag\{Co(CO)_4\}_2]^-$ anions (Figure 3). The structure of $[Ag\{Co(CO)_4\}_2]^-$ has been recently reported as a $[NEt_4]^+$ salt,[30] showing very similar geometry and structural parameters. It closely resembles the related $[Cu\{Co(CO)_4\}_2]^-$ and $[Au\{Co(CO)_4\}_2]^-$ species.[1,31−33] The Ag−Co distances [2.5375(4) and 2.5500(4) Å] are similar to that of **2**

https://doi.org/10.1021/acs.organomet.1c00363
Organometallics 2021, 40, 2724−2735

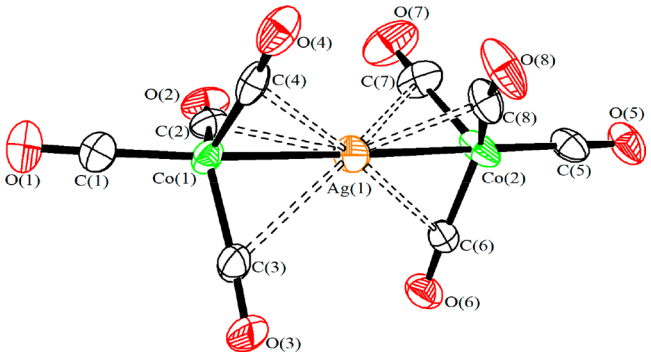

Figure 3. Molecular structure of the $[Ag\{Co(CO)_4\}_2]^-$ anion present in $[Ag(IMes)_2][Ag\{Co(CO)_4\}_2]$ (**9**). Thermal ellipsoids are at the 50% probability level. Ag···C(O) contacts [2.42−2.83 Å] are represented as fragmented lines (green Co; orange Ag; red O; gray C). Main bond distances (Å) and angles (deg): Co−Ag 2.5375(4) and 2.5500(4), Co−C(O) 1.763(3)−1.783(3), Co−Ag−Co 175.082(17).

[2.5344(3) Å] and slightly shorter than in the neutral tetramer $[Ag_4\{Co(CO)_4\}_4]$ [2.59 Å].[34] The Ag(I) ion displays a linear coordination and the two Co-centers adopt both a TBP geometry as previously found also in $[Au\{Co(CO)_4\}_2]^-$.[33] Regarding $[Cu\{Co(CO)_4\}_2]^-$, four crystal structures have been previously reported in the literature with miscellaneous cations,[1,31,32] comprising that of **8** (space group $P2_1/n$). During this work we have also isolated a second polymorph of **8** (space group $C2/c$). In all of these salts, the two Co-centers of $[Cu\{Co(CO)_4\}_2]^-$ adopt a TBP coordination (TBP−TBP isomer), except in the $[PPN][Cu\{Co(CO)_4\}_2]$ salt, where one Co center is TBP and the second one displays a tetrahedral coordination of the four CO ligands, with Cu capping one edge of the $Co(CO)_4$ tetrahedron (TBP−Td isomer). In all of the other structurally characterized salts, the $[M\{Co(CO)_4\}_2]^-$ anion adopts the TBP−TBP geometry with the two $Co(CO)_4$ fragments in a staggered conformation. An exception is represented by $[Cu(dmpe)_2][Cu\{Co(CO)_4\}]$,[31] which possesses the TBP−TBP structure, but within the unit cell there is one anion adopting the most common staggered conformation, whereas a second anion displays an unique eclipsed conformation. A detailed experimental and computational study on the different isomers of $[M\{Co(CO)_4\}_2]^-$ has been recently published.[30]

Compounds **1**−**3** and **7**−**9** are thermally stable, and they do not react with oxidizing or reducing agents (e.g., I_2, $HBF_4\cdot Et_2O$, Na/naphtalene, Cp_2Ni, $[Cp_2Fe]^+$, PPh_3, and Me_3NO). By contrast, the thermal reactions of **2** and **8** with $Co_2(CO)_8$ in refluxing THF for 300 min afforded traces of $[HIPr]_2[Ag_2\{Co(CO)_4\}_4]$ (**11**) and $[Co_4(CO)_8(\mu\text{-}\eta^7\text{-IMes})]$ (**12**), respectively.

Compound **11** consists of an ionic packing of $[HIPr]^+$ cations and $[Ag_2\{Co(CO)_4\}_4]^{2-}$ anions (Figure 4). The latter anion has been recently characterized as miscellaneous salts,[30] whereas no Cu- and Au-related species are known. It may be viewed as a dimer of $[Ag\{Co(CO)_4\}_2]^-$, as previously described. The Ag−Ag contact [2.8631(3) Å] is indicative of an argentophilic interaction[35] as found in other salts containing the same $[Ag_2\{Co(CO)_4\}_4]^{2-}$ anion.[30] $[Ag_2\{Co(CO)_4\}_4]^{2-}$ contains two types of $Co(CO)_4$ group, indicated as Co_t (terminal) and Co_b (bringing). As expected, the Co_t−Ag contact [2.6451(3)Å] is shorter than Co_b−Ag [2.7510(3) and 2.8494(3) Å]. Moreover, the Co_t−Ag distance of $[Ag_2\{Co(CO)_4\}_4]^{2-}$ is longer than in **2** and **9**, in view of the fact that Ag displays coordination number of two in **2** and **9** and three (four considering also the Ag−Ag contact) in **11**. Indeed, the Ag−Co contact [2.75 Å] in the mononuclear complex $Co(CO)_4\{AgAs_3(CH_3)_5(C_6H_4)_2\}$, that contains a Ag center strongly bound to three As atoms (Ag coordination number of four), is even longer than that in **11**.[26]

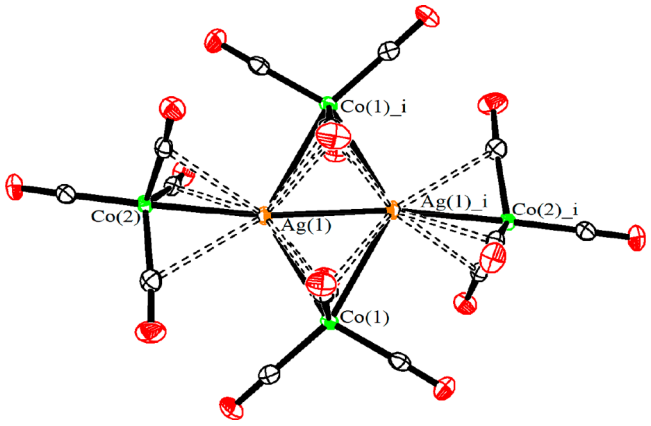

Figure 4. Molecular structure of the $[Ag_2\{Co(CO)_4\}_4]^{2-}$ anion present in $[HIPr]_2[Ag_2\{Co(CO)_4\}_4]$ (**11**). Thermal ellipsoids are at the 50% probability level. Ag···C(O) contacts [2.60−2.99 Å] are represented as fragmented lines (green, Co; orange, Ag; red, O; gray, C). Main bond distances (Å) and angles (deg): Ag−Ag 2.8631(3), Co_t−Ag 2.6451(3), Co_b−Ag 2.7510(3) and 2.8494(3), Co_t−C(O) 1.757(2)−1.782(2), Co_b−C(O) 1.784(2)−1.789(2), Co_t−Ag−Ag 171.812(10), Ag−Co_b−Ag 61.462(8).

Neutral cluster **12** may be viewed as a derivative of the tetrahedral cluster $Co_4(CO)_{12}$, where four CO ligands have been replaced by a $\mu\text{-}\eta^7$-IMes ligand (Figure 5). The cluster

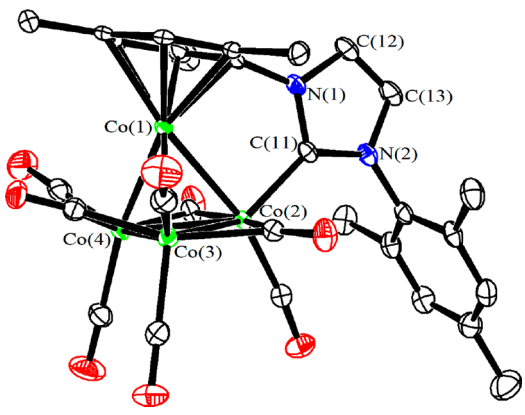

Figure 5. Molecular structure of $[Co_4(CO)_8(\mu\text{-}\eta^7\text{-IMes})]$ (**12**). Thermal ellipsoids are at the 50% probability level. Hydrogen atoms have been omitted for clarity (green, Co; blue, N; red, O; gray, C). Main bond distances (Å): Co−$C_{carbene}$ 1.968(2), Co−η^6-C_6 2.038(2)−2.167(2), Co−$CO_{terminal}$ 1.773(3)−1.792(3), Co−$CO_{bridging}$ 1.886(2)−1.976(2), Co−Co 2.4275(4)−2.4954(5).

possesses a tetrahedral Co_4 core with three μ-CO ligands on the basal Co_3 triangle. Within this triangle, two Co atoms are bound to one axial and one equatorial terminal CO, whereas the third Co is bound to one axial CO and the $C_{carbene}$ of IMes in the equatorial position. One aromatic ring of IMes is η^6-bound to the fourth Co atom. The $\mu\text{-}\eta^7$-coordination (six aromatic carbons plus one carbene carbon atom) is unprecedented for IMes, but it has been previously reported

https://doi.org/10.1021/acs.organomet.1c00363
Organometallics 2021, 40, 2724−2735

for other NHC ligands possessing aromatic substituents,[36−39] including the $HRu_7(CO)_{17}(\mu\text{-}\eta^7\text{-NHC})$ cluster [NHC = $C_3H_2(Me)(Ph)$].[40] It is well-known that $Co_2(CO)_4$ is thermally transformed into $Co_4(CO)_{12}$.[41] In the presence of IMes, the latter may lose four further CO ligands, resulting in **12**.

2.2. Ammonia Borane Dehydrogenation. Bimetallic Co−M−NHC complexes **1**−**3** and **7**−**9** have been tested as catalysts for the dehydrogenation of ammonia borane (AB) in THF as solvent. In view of the results discussed in section 2.1, compounds **1**−**3** and **7** are present in THF mainly (or solely) as neutral species $[Co(CO)_4\{M(NHC)\}]$, whereas **8** and **9** are ionic species $[M(NHC)_2][M\{Co(CO)_4\}_2]$. For comparison, also bimetallic Fe−M−NHC complexes have been tested, that is, $[Fe(CO)_4\{M(NHC)\}_2]$. Moreover, in order to verify the relevance of the bimetallic nature of these species in catalysis, also related homometallic species have been tested under similar experimental conditions, that is, M(NHC)Cl and $Na[Co(CO)_4]$. All these catalysts have been preliminarily tested by NMR at 298 or 323 K. In a typical test, the catalyst, AB, and THF were mixed in an oven-dried NMR tube containing a capillary with $BF_3{\cdot}Et_2O$ as reference, and the sample was maintained at 298 and 323 K. The disappearance of AB with time has been monitored by ^{11}B NMR comparing the integral of the resonance of AB with that of $BF_3{\cdot}Et_2O$ The results are summarized in Tables 2 and 3.

Table 2. Catalytic Dehydrogenation of AB at 298 K Monitored by ^{11}B NMR Spectroscopy[a]

		AB conversion (%) by ^{11}B NMR		
catalyst	solvent	1 h	4 h	24 h
none	THF	0	0.3	10
1	THF	60	94	100
1	diglyme	66	-	100
2	THF	0	0	3
3	THF	0	0	33
7	THF	0	0	9
8	THF	1	1	1
9	THF	0	5	7
$[Fe(CO)_4\{Cu(IPr)\}_2]$	THF	39	43	80
$[Fe(CO)_4\{Au(IPr)\}_2]$	THF	28	35	43
$[Fe(CO)_4\{Cu(IMes)\}_2]$	THF	17	28	39
$[Fe(CO)_4\{Au(IMes)\}_2]$	THF	33	29	32
Cu(IPr)Cl	THF	32	27	26
Cu(IMes)Cl	THF	13	23	18
$Na[Co(CO)_4]$	THF	0	0	0

[a]Catalyst load 5% mol/mol.

Complex **1** displays the complete conversion of AB after 24 h at 298 K, and after 4 h, the conversion is already 94%. The catalytic performance of **1** significantly decreases at 323 K. Conversely, $[Fe(CO)_4\{Cu(IPr)\}_2]$ displays an opposite trend: the conversion is 80% after 24 h at 298 K and increases up to 100% at 323 K. Related homometallic species are almost inactive. Bimetallic Co−Ag complexes such as **2** and **9** are inactive at 298 K, and only the latter displays 47% conversion after 24 h at 323 K. Co−Au and Fe−Au are less active compared to Co−Cu and Fe−Cu complexes. Moreover, their catalytic performances increase significantly with temperature.

According to these preliminary studies, the best catalyst seems to be **1**. Indeed, **1** displays the complete conversion of AB after 24 h at 298 K, and after 4 h, the conversion is already 94% (Figure 6).

Table 3. Catalytic Dehydrogenation of AB at 323 K Monitored by ^{11}B NMR Spectroscopy[a]

		AB conversion (%) by ^{11}B NMR		
catalyst	solvent	1 h	4 h	24 h
none	THF	0	8	21
1	THF	45	49	70
2	THF	0	0	0
3	THF	0	7	78
7	THF	3	18	52
8	THF	7	18	54
9	THF	49	50	47
$[Fe(CO)_4\{Cu(IPr)\}_2]$	THF	18	43	100
$[Fe(CO)_4\{Au(IPr)\}_2]$	THF	23	24	69
$[Fe(CO)_4\{Cu(IMes)\}_2]$	THF	21	32	70
$[Fe(CO)_4\{Au(IMes)\}_2]$	THF	23	22	31
$Na[Co(CO)_4]$	THF	14	13	35

[a]Catalyst load 5% mol/mol.

In order to obtain further information on the catalytic AB dehydrogenation promoted by **1**, the reaction was monitored by *in situ* IR spectroscopy. The experiments were conducted in a FT-IR cell with CaF_2 windows and in a 200 mL batch reactor by employing the same concentration of reagents employed in the NMR tube experiments.

In Figure 7, the IR spectrum of the substrate and the catalyst before the catalytic reaction are reported. As far as AB is concerned, its spectrum presents three bands at 3310, 3239, and 3180 cm^{-1} due to the different N−H stretching modes and four bands at 2356, 2317, 2275, and 2220 cm^{-1} referred to the B−H stretching modes.[42−45] In the ν_{CO} region, it is possible to observe four bands belonging to the catalyst **1** (2046, 1966, 1943, and 1924 cm^{-1}).

During the reaction, the consumption of AB is followed by the decrease in intensity of the bands relative to the N−H and B−H stretching modes in the regions of 3400−3100 and 2400−2200 cm^{-1}, respectively. The dehydrogenation of the substrate is promoted by the catalyst which during the reaction evolves in a deactivated form. This transformation is accompanied by the disappearance of the four ν_{CO} bands of **1** and the growth of a band centered at 1892 cm^{-1}, attributable to the monoanion $[Co(CO)_4]^-$ (Figure 8). This trend was observed in both the two reaction systems, that is, the reactor and the IR cell. The reaction progress in the reactor is highlighted with a light purple solid line (start of reaction) and a black dashed and dotted line (end of reaction). It is noteworthy that the evolution of the catalyst toward the deactivated form is slow, and after 10 h, it is still incomplete (Figure 8, black dashed and dotted line). Similarly, the conversion of AB is not complete after the same reaction time.

To better highlight the trend observed in the reactor and to see if there are other carbonyl species originating from the catalyst, the spectra recorded in the IR cell, after subtraction of the first spectrum, were analyzed in the CO stretching region (Figure 9). The negative bands at 2046, 1966, 1943, and 1924 cm^{-1} and the concomitant growth of the band at 1892 cm^{-1} confirm the transformation of the catalyst **1** into $[Co(CO)_4]^-$.

The composition of the gas in the reactor head space was analyzed at different time intervals. These analyses allowed to quantify the amount of H_2 evolved during the dehydrogenation

https://doi.org/10.1021/acs.organomet.1c00363
Organometallics 2021, 40, 2724−2735

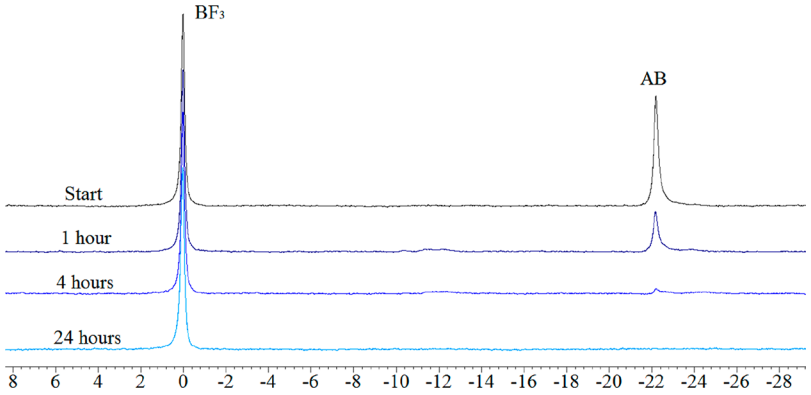

Figure 6. ^{11}B NMR spectra acquired during the catalytic dehydrogenation of AB with **1** in THF at 298 K. Catalyst load 5% mol/mol. A capillary with a $BF_3{\cdot}Et_2O$ is used as reference.

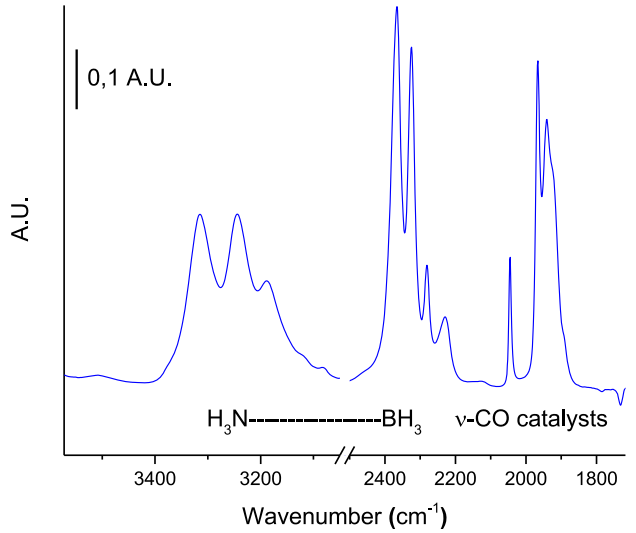

Figure 7. FT-IR spectrum of a solution of NH_3BH_3 and **1** in THF, after subtraction of the THF spectrum.

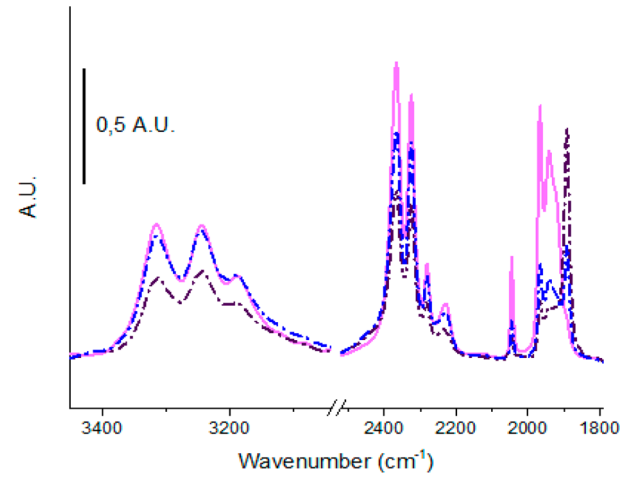

Figure 8. FT-IR spectra after subtraction of the THF spectrum. The IR spectra were recorded by monitoring the dehydrogenation of AB catalyzed by **1**. Solid light purple line: spectrum recorded at the beginning of the reaction. Intermediate dashed and dotted blue line: spectrum recorded after 5 h of reaction in the reactor. Dashed and dotted black line: spectrum recorded after 10 h of reaction in the reactor.

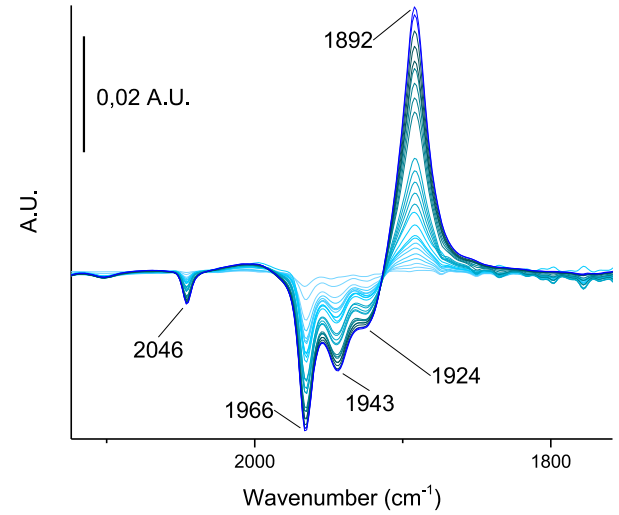

Figure 9. FT-IR spectra after subtraction of the first spectrum at the beginning of reaction. The IR spectra were recorded by monitoring the dehydrogenation of AB in the presence of **1**. From light blue to blue lines: spectra recorded over time in the IR cell.

of AB. After 300 min of reaction, 0.63 equiv of H_2 referred to the initial moles of AB were formed (Figure 10, black line). Hydrogen production shows a maximum after ca. 40 min (Figure 10, blue line). Then, the reaction rate rapidly decreases

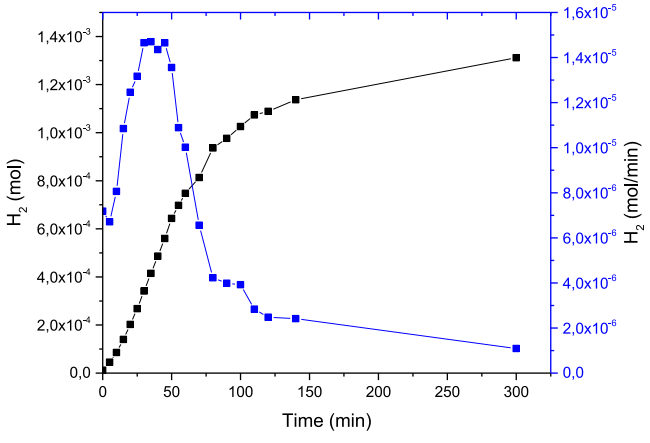

Figure 10. Moles of H_2 produced by reacting AB with **1** in the reactor (black line) and moles of H_2 formed per minute (blue line).

https://doi.org/10.1021/acs.organomet.1c00363
Organometallics 2021, 40, 2724−2735

in the next 10 min; after this point, the reaction proceeds with a very slow rate. Further studies are required in order to rationalize and explain this behavior.

The formation of a white precipitate is observed during the catalytic reaction. This solid has been recovered by filtration, stored in air at room temperature, and analyzed by powder X-ray diffraction (Figure 11, red line). The solid is a mixture of

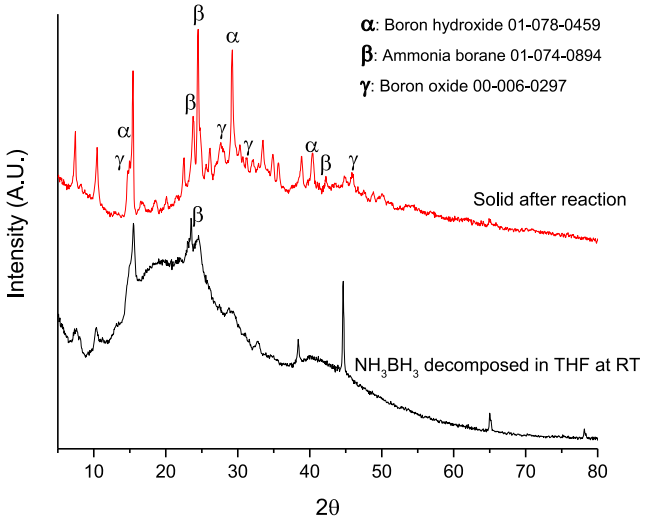

Figure 11. Diffraction pattern of the solid produced during the reaction stored at room temperature in air (red line) and AB decomposed in THF at room temperature in air.

crystalline and amorphous phases, whose identification is not so straightforward. The crystalline phases present in the mixture can be tentatively assigned to unconverted AB, boron hydroxide, and boron oxide. The absence of nitrogen-containing compounds suggests that N−B bonds are broken during reaction. This point is further corroborated by the presence of ammonia in the head space of the reactor at the end of the catalytic process.[25]

For the sake of comparison, the diffraction pattern of the solid obtained from the decomposition of pure AB under similar conditions (at room temperature, in THF under air) is reported (Figure 11, black line). Under these conditions, AB decomposed, mostly affording an amorphous solid. Moreover, the peaks relative to the crystalline phases do not match with the peaks of the solid produced during the catalytic reaction.

2.3. Computational Investigations. DFT computations have been performed to provide information on structure, IR spectroscopy and thermodynamics of Co−M carbonyl clusters that could support experimental evidence.

The computed geometry of **1** in the gas phase is close to the X-ray one, featuring equatorial COs with carbons partially pulled toward Cu due to Cu···C(O) interactions (see section 2.1). This implies that the Co−C−O angles are also not exactly 180° (i.e., ∼176°) for **1** in vacuum, indicating that crystal packing interactions do not have a significant effect on the structural features of isolated complex **1**. In order to get further insights into the nature of the most relevant interactions in complexes **1**−**3**, a natural bond order (NBO) analysis was carried out, and the Wiberg bond index (WBI) was computed,[46] suggesting that the Co−M bonds do not feature any strong covalent character, in line with their lability and with the similarities of the IR spectra of the complexes (i.e., carbonyl groups vibrational frequencies are not dramatically affected by the M type). Nevertheless, an increasing covalent character was found going from Cu to Au (with WBIs of 0.26, 0.31, and 0.38 for **1**, **2**, and **3**, respectively) and from IPr to less hindered IMes ligands (with WBIs of 0.30, 0.32, and 0.39 for **5**, **6**, and **7**, respectively). Moreover, natural atomic charges[47] suggest the presence of electrostatic interactions between negatively charged Co and positively charged M centers, confirming the overall electrostatic nature of these complexes.

Regarding the weak Cu···C(O) interactions, while as expected they do not feature any strong covalent character, the second-order perturbation theory analysis of the Fock matrix in NBO basis of complex **1** revealed significant interactions between both the 3d and 4s Cu orbitals and the antibonding π^* orbitals of equatorial carbonyl groups. Moreover, the inspection of occupied molecular orbitals of **1** indicated the presence of an occupied frontier orbital (HOMO−2) associated to these interactions, as shown in Figure 12. A semibridging character for the equatorial COs can

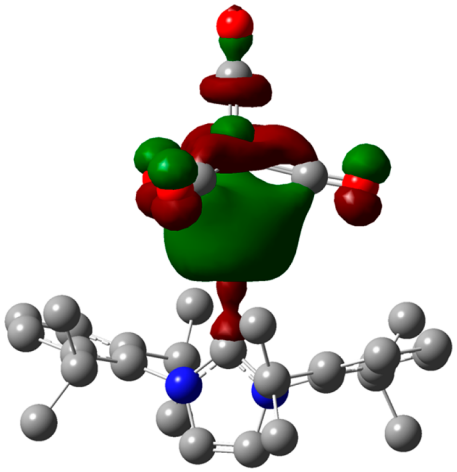

Figure 12. Occupied molecular orbital (HOMO−2) of complex **1**, involving Cu orbitals and π^* orbitals of equatorial CO groups.

be assigned computing the "bridge asymmetry" parameter (α) and the WBIs for Cu···C(O), as already reported by Mankad et al.[48] The computed α values for complex **1** are in the range of 0.31−0.32, and the WBIs are within 0.12−0.13, falling in the category of weak semibridging interactions.[48]

The simulated IR spectrum of **1** reproduces the experimental spectra recorded in toluene (Figure S1) and THF (Figure S16), which features, as previously described, a sharp (characteristic) band at around 2040 cm^{-1} and a much broader band at 1950 cm^{-1}. While the former peak is associated to CO stretchings involving (coupled) axial and equatorial carbonyls, the broad band is related to stretchings of just equatorial CO groups. As mentioned above, the variation of M does not imply significant changes in the IR spectra of complexes **1**−**3**, with theoretical predictions corroborating the experimental evidence of almost identical spectra for **1** and **2**, while the IR spectrum of **3** features a slight rigid blueshift of both the sharp (ca. + 5 cm^{-1}) and broad (ca. + 10 cm^{-1}) bands (Figure S17). For NHC = IMes, the simulated IR spectra do not show critical changes with respect to those with NHC = IPr (Figure S18). This observation and the fact that our previously reported simulated and experimental IR spectra of the ionic species[30] featured a sharp band red-shifted by ca. 40

https://doi.org/10.1021/acs.organomet.1c00363
Organometallics 2021, 40, 2724−2735

Scheme 2. Equilibria of Formation (ΔG_1) and Dissociation (ΔG_2) of the Ionic $[M(NHC)_2]^+[M\{Co(CO)_4\}_2]^-$ Species

$$2\,[Co(CO)_4\{M(NHC)\}] \underset{}{\overset{\Delta G_1}{\rightleftharpoons}} [M(NHC)_2]^+[M\{Co(CO)_4\}_2]^- \overset{\Delta G_2}{\rightleftharpoons} [M(NHC)_2]^+ + [M\{Co(CO)_4\}_2]^-$$

cm^{-1} as compared to the spectra of the neutral species (i.e., those reported in this work) shows an overall good agreement between experimental and theoretical IR spectra that strongly supports the above discussion on the detection of ionic species in the mixtures (see section 2.1).

Since the $[Co(CO)_4\{M(NHC)\}]$ formations are spontaneous, due to the NaCl precipitation previously described, we focused our DFT investigations on the thermodynamics of the subsequently formed ionic species $[M(NHC)_2]^+$ and $[M\{Co(CO)_4\}_2]^-$ (see Scheme 1), in order to gather more information on the behavior of these ionic pairs in solution. As shown in Scheme 2 and Table 4, we computed the free energies of formation (ΔG_1) and dissociation (ΔG_2) of the ionic $[M(IPr)_2]^+[M\{Co(CO)_4\}_2]^-$ species, looking at the influence of M and solvent dielectric. Considering a small dielectric constant (ε = 7, i.e., a solvent with low polarity), we observed that formation of tight ionic pairs is energetically costly for M = Cu (ΔG_1 = 11.9 kcal/mol) if compared to M= Ag and Au, whose ΔG_1 is halved. By increasing the solvent polarity (to ε = 78), this trend is even more marked, with a ΔG_1 similar to low dielectric for Cu. For Ag and Au, it tends to isoergonicity, and values for Ag are generally lower than for Au. These results are consistent with the experimental IR spectra, since spectral features associated to ionic species have never been detected in the case of Cu (Figures S1 and S16). For Au, only a spectral shoulder of the sharp band at 2045 cm^{-1} could be identified in dmso (Figure S3), and for Ag, a clear peak at 2025 cm^{-1} is recorded (Figure S2).

Table 4. DFT Free Energies of Formation (ΔG_1) and Dissociation (ΔG_2) of the Ionic $[M(IPr)_2]^+[M\{Co(CO)_4\}_2]^-$ Species (M = Cu, Ag, and Au) and Considering Two Different Solvent Dielectric Constants (ε)

	ε = 7		ε = 78	
	ΔG_1 (kcal/mol)	ΔG_2 (kcal/mol)	ΔG_1 (kcal/mol)	ΔG_2 (kcal/mol)
Cu (**1**)	11.9	4.2	12.0	0.1
Au (**3**)	6.3	5.4	2.2	1.3
Ag (**2**)	5.7	5.1	0.8	1.1

The dissociation reactions of $[M(IPr)_2]^+[M\{Co(CO)_4\}_2]^-$ tight ionic pairs are endergonic in solvents with either low or high polarity, while the corresponding free energies values (ΔG_2) are small enough (around 5 or 1 kcal/mol, respectively) to expect that dissociated species can be still easily formed in the solution mixtures.

Finally, for complex **5** (with NHC = IMes) we also computed the ΔG_1 for the formation of $[Cu(IMes)_2]^+[Cu\{Co(CO)_4\}_2]^-$ species, which resulted to be an exergonic spontaneous process (by −2.4 kcal/mol), in contrast with the large positive ΔG_1 computed for NHC = IPr (i.e., complex **1**, see Table 4), corroborating the experimental evidence that IMes ligands generally favor the formation of ionic species in the reaction mixtures, due to the steric properties of the $[M(NHC)_2]^+$ cation.

3. CONCLUSIONS

Heterometallic complexes **1**−**10** have been prepared starting from $Na[Co(CO)_4]$ and M(NHC)Cl. Neutral $[Co(CO)_4\{M(NHC)\}]$ and ionic $[M(NHC)_2][M\{Co(CO)_4\}_2]$ species may be obtained, depending on the nature of M and NHC. In some cases, both species are present at the same time in solution. The bulkier IPr ligand seems to be the best one in order to stabilize heterometallic Co−M(NHC) bonds, as previously found for related Fe−M(NHC) bonds.[9−13] Such heterometallic Co−M(NHC) and Fe−M(NHC) carbonyl complexes have been tested as catalysts for AB dehydrogenation. The best results have been obtained using $[Co(CO)_4\{Cu(IPr)\}]$ (**1**) and $[Fe(CO)_4\{Cu(IPr)\}_2]$, which both contain the Cu(IPr) fragment. This might be related to the higher capacity of Cu compared to that of Ag and Au to stabilize M−H (hydride) interactions.[49] Indeed, AB contains both hydridic (B−H) and protic (N−H) hydrogens, and its activation is likely to proceed through the concomitant interactions of B−H with the positively charged Cu(IPr) fragment and of N−H with the negatively charged $Co(CO)_4$ or $Fe(CO)_4$ fragment. Further work is required in order to better elucidate the mechanism of the catalytic process both from an experimental and theoretical point of view.

4. EXPERIMENTAL SECTION

4.1. General Experimental Procedures. All reactions and sample manipulations were carried out using standard Schlenk techniques under nitrogen and in dried solvents. All the reagents were commercial products (Aldrich) of the highest purity available and used as received, except $Na[Co(CO)_4]$[50] and M(NHC)Cl (M = Cu, Ag, and Au; NHC = IMes and IPr)[51] which were prepared according to the literature. Analyses of C, H, and N were obtained with a Thermo Quest Flash EA 1112NC instrument. IR spectra were recorded on a PerkinElmer Spectrum One interferometer in CaF_2 cells. ^1H, $^{13}C\{^1H\}$, and ^{11}B NMR measurements were performed on a Varian Mercury Plus 400 MHz instrument. The proton and carbon chemical shifts were referenced to the nondeuterated aliquot of the solvent. The boron chemical shifts were referenced to $BF_3{\cdot}Et_2O$ using an internal capillary.

The XRD powder analysis was carried out using a PANalytical X'Pert diffractometer equipped with a copper anode (Cu Kα, λ = 0.15418 nm) and a fast X'Celerator detector. A 2θ range of 5−80° was investigated, using a step size of 0.1° and a time per step of 2 s.

4.2. Synthesis of [Co(CO)$_4${Cu(IPr)}] (1). $Na[Co(CO)_4]$ (0.410 g, 2.12 mmol) and Cu(IPr)Cl (1.06 g, 2.17 mmol) were charged in a Schlenk tube under a nitrogen atmosphere, and THF (15 mL) was added. The mixture was stirred for 20 min at room temperature, and then, the solvent removed under reduced pressure. The crude product was extracted in toluene (15 mL), and crystals of **1** were obtained by slow diffusion of *n*-pentane (30 mL) at −20 °C (yield 1.02 g, 76%). These crystals displayed the same unit cell reported in the literature.[1]

$C_{31}H_{36}CuCoN_2O_4$ (622.13): calcd (%): C 59.79, H 5.83, N 4.50. Found: C 60.08, H 5.67, N 4.33. IR (nujol, 293 K) ν_{CO}: 2039 (mw), 1961 (m), 1927 (ms) cm^{-1}. IR (toluene, 293 K) ν_{CO}: 2041 (s), 1964 (s), 1934 (s), 1917 (sh) cm^{-1}. IR ($CHCl_3$, 293 K) ν_{CO}: 2041 (s), 1962 (s), 1936 (s), 1918 (sh) cm^{-1}. IR (CH_2Cl_2, 293 K) ν_{CO}: 2041 (s), 1960 (s), 1935 (s), 1913 (sh) cm^{-1}. IR (THF, 293 K) ν_{CO}: 2039 (ms), 1961 (s), 1935 (s), 1915 (sh) cm^{-1}. IR (acetone, 293 K) ν_{CO}: 2040 (ms), 1961 (s), 1937 (s), 1913 (sh) cm^{-1}. IR (CH_3CN, 293 K) ν_{CO}: 2041 (w), 1962 (m), 1935 (m), 1892 (s) cm^{-1}. IR (dmso, 293 K) ν_{CO}: 2039 (w), 1957 (m), 1934 (m), 1889 (s) cm^{-1}. ^1H NMR (C_6D_6, 298 K): δ 7.23 (t, $^2J_{HH}$ = 7.5 Hz, 2H, CH_{Ar}), 7.08 (d, $^2J_{HH}$ =

https://doi.org/10.1021/acs.organomet.1c00363
Organometallics 2021, 40, 2724−2735

7.5 Hz, 4H, CH_{Ar}), 6.29 (s, 2H, CH_{imid}), 2.59 (sept, $^2J_{HH}$ = 6.3 Hz, 4H, $CH(CH_3)_2$), 1.38 (d, $^2J_{HH}$ = 5 Hz, 12H, $CH(CH_3)_2$), 1.05 (d, $^2J_{HH}$ = 5 Hz, 12H, $CH(CH_3)_2$). $^{13}C\{^1H\}$ NMR (C_6D_6, 298 K): δ 160.3 (C−Cu), 145.4, 134.9, 131.0, 124.5, 122.7 (C_{Ar} and CH_{imid}), 29.0 ($CH(CH_3)_2$), 24.5, 24.2 ($CH(CH_3)_2$). No peak corresponding to bound CO was located.

4.3. Synthesis of [Co(CO)$_4${Ag(IPr)}] (2). Na[Co(CO)$_4$] (0.200 g, 1.04 mmol) and Ag(IPr)Cl (0.440 g, 1.04 mmol) were charged in a Schlenk tube under a nitrogen atmosphere, and THF (15 mL) was added. The mixture was stirred for 60 min at room temperature, and then, the solvent was removed under reduced pressure. The crude product was extracted in toluene (15 mL), and crystals of **2** were obtained by slow diffusion of *n*-pentane (30 mL) at −20 °C (yield 0.45 g, 65%).

$C_{31}H_{36}AgCoN_2O_4$ (667.42): calcd (%): C 55.85, H 5.45, N 4.20. Found: C 55.61, H 5.74, N 4.49. IR (nujol, 293 K) ν_{CO}: 2037 (s), 1958 (s), 1925 (s) cm^{-1}. IR (toluene, 293 K) ν_{CO}: 2040 (s), 1962 (s), 1933 (s) cm^{-1}. IR ($CHCl_3$, 293 K) ν_{CO}: 2040 (s), 1959 (sh), 1937 (s) cm^{-1}. IR (CH_2Cl_2, 293 K) ν_{CO}: 2040 (ms), 1958 (s), 1935 (s) cm^{-1}. IR (THF, 293 K) ν_{CO}: 2039 (s), 2024 (w), 1958 (s), 1935 (s) cm^{-1}. IR (acetone, 293 K) ν_{CO}: 2039 (s), 1959 (s), 1936 (s) cm^{-1}. IR (CH_3CN, 293 K) ν_{CO}: 2041 (m), 1959 (s), 1934 (s), 1893 (mw) cm^{-1}. IR (dmso, 293 K) ν_{CO}: 2038 (m), 1955 (s), 1935 (s), 1890 (m) cm^{-1}. ^1H NMR (CD_2Cl_2, 298 K): δ 7.67 (s, 2H, CH_{imid}), 7.49 (t, $^2J_{HH}$ = 7.8 Hz, 2H, CH_{Ar}), 7.36 (d, $^2J_{HH}$ = 7.8 Hz, 4H, CH_{Ar}), 2.65 (sept, $^2J_{HH}$ = 6.8 Hz, 4H, $CH(CH_3)_2$), 1.39 (d, $^2J_{HH}$ = 6.8 Hz, 12H, $CH(CH_3)_2$), 1.31 (d, $^2J_{HH}$ = 6.8 Hz, 12H, $CH(CH_3)_2$). $^{13}C\{^1H\}$ NMR (CD_2Cl_2, 298 K): δ 205.8 (br, CO), 185.3 (C−Ag, $^1J_{C-Ag}$ = 234 and 202 Hz), 144.8, 134.2, 129.5, 123.2, 123.1 (C_{Ar} and CH_{imid}), 27.9 ($CH(CH_3)_2$), 23.1, 22.4 ($CH(CH_3)_2$).

4.4. Synthesis of [Co(CO)$_4${Au(IPr)}] (3). Na[Co(CO)$_4$] (0.190 g, 0.984 mmol) and Au(IPr)Cl (0.610 g, 0.984 mmol) were charged in a Schlenk tube under a nitrogen atmosphere, and THF (15 mL) was added. The mixture was stirred for 30 min at room temperature, and then the solvent was removed under reduced pressure. The crude product was extracted in toluene (15 mL), and crystals of **3** were obtained by slow diffusion of *n*-pentane (30 mL) at −20 °C (yield 0.58 g, 78%).

$C_{31}H_{36}AuCoN_2O_4$ (756.51): calcd (%): C 49.20, H 4.80, N 3.70. Found: C 49.36, H 4.52, N 3.94. IR (nujol, 293 K) ν_{CO}: 2044 (s), 1969 (s), 1939 (s) cm^{-1}. IR (toluene, 293 K) ν_{CO}: 2048 (s), 1973 (s), 1949 (s) cm^{-1}. IR ($CHCl_3$, 293 K) ν_{CO}: 2047 (s), 1970 (sh), 1952 (s) cm^{-1}. IR (CH_2Cl_2, 293 K) ν_{CO}: 2047 (s), 1968 (s), 1951 (s) cm^{-1}. IR (acetone, 293 K) ν_{CO}: 2046 (s), 1969 (s), 1952 (s) cm^{-1}. IR (CH_3CN, 293 K) ν_{CO}: 2048 (s), 1971 (s), 1950 (s) cm^{-1}. IR (dmso, 293 K) ν_{CO}: 2045 (s), 1964 (s), 1949 (s), 1892 (m) cm^{-1}. ^1H NMR (CD_2Cl_2, 298 K): δ 7.53 (t, $^2J_{HH}$ = 7.8 Hz, 2H, CH_{Ar}), 7.34 (d, $^2J_{HH}$ = 7.8 Hz, 4H, CH_{Ar}), 7.27 (s, 2H, CH_{imid}), 2.63 (sept, $^2J_{HH}$ = 6.8 Hz, 4H, $CH(CH_3)_2$), 1.35 (d, $^2J_{HH}$ = 6.8 Hz, 12H, $CH(CH_3)_2$), 1.25 (d, $^2J_{HH}$ = 6.8 Hz, 12H, $CH(CH_3)_2$). $^{13}C\{^1H\}$ NMR (CD_2Cl_2, 298 K): δ 207.6 (br, CO), 187.2 (C−Au), 145.7, 134.1, 130.4, 124.0, 122.8 (C_{Ar} and CH_{imid}), 28.8 ($CH(CH_3)_2$), 23.9, 23.7 ($CH(CH_3)_2$).

4.5. Synthesis of [Cu(IMes)$_2$][Cu{Co(CO)$_4$}$_2$] (8). Na[Co(CO)$_4$] (0.410 g, 2.12 mmol) and Cu(IMes)Cl (0.880 g, 2.18 mmol) were charged in a Schlenk tube under a nitrogen atmosphere, and THF (15 mL) was added. The mixture was stirred for 20 min at room temperature, and then the solvent was removed under reduced pressure. The crude product was extracted in toluene (15 mL), and crystals of **8** were obtained by slow diffusion of *n*-pentane (30 mL) at −20 °C (yield 0.59 g, 50%). The crystals obtained are a polymorph (space group *C*2/*c*) of the previously reported structure (space group $P2_1/n$).[1]

$C_{50}H_{48}Cu_2Co_2N_4O_8$ (1077.86): calcd (%): C 55.76, H 4.50, N 5.21. Found: C 55.35, H 4.84, N 5.04. IR (THF, 293 K) ν_{CO}: 2039 (w), 2022 (m), 1950 (s), 1936 (s), 1885 (s) cm^{-1}. ^1H NMR (C_6D_6, 298 K): δ 6.74 (s, 4H, CH_{Ar}), 5.96 (s, 2H, CH_{imid}), 2.07 (s,6H, CH_3), 1.96 (s, 12H, CH_3). $^{13}C\{^1H\}$ NMR (C_6D_6, 298 K): δ 178.8 (C−Cu), 139.6, 135.1, 134.5, 129.5, 121.4, (C_{Ar} and CH_{imid}), 17.3, 16.8 (CH_3). No peak corresponding to bound CO was located. During the several attempts to crystallize **8**, a few crystals of [Cu(IMes)$_2$][Co(CO)$_4$] were also obtained.

4.6. Synthesis of [Ag(IMes)$_2$][Ag{Co(CO)$_4$}$_2$] (9). Na[Co(CO)$_4$] (0.200 g, 1.04 mmol) and Ag(IMes)Cl (0.370 g, 1.04 mmol) were charged in a Schlenk tube under a nitrogen atmosphere, and THF (15 mL) was added. The mixture was stirred for 60 min at room temperature, and then the solvent was removed under reduced pressure. The crude product was extracted in toluene (15 mL), and crystals of **9** were obtained by slow diffusion of *n*-pentane (30 mL) at −20 °C (yield 0.31 g, 51%).

$C_{50}H_{48}Ag_2Co_2N_4O_8$ (1166.52): calcd (%): C 51.55, H 4.16, N 4.81. Found: C 51.89, H 3.89, N 4.52. IR (nujol, 293 K) ν_{CO}: 2022 (s), 1934 (s) cm^{-1}. IR (toluene, 293 K) ν_{CO}: 2040 (m), 2025 (m), 1959 (s), 1935 (s) cm^{-1}. IR ($CHCl_3$, 293 K) ν_{CO}: 2039 (mw), 2025 (w), 1956 (sh), 1937 (s) cm^{-1}. IR (CH_2Cl_2, 293 K) ν_{CO}: 2038 (w), 2026 (m), 1937 (s) cm^{-1}. IR (THF, 293 K) ν_{CO}: 2038 (w), 2025 (m), 1939 (s), 1887 (w) cm^{-1}. IR (acetone, 293 K) ν_{CO}: 2038 (w), 2027 (m), 1944 (s), 1940 (s), 1892 (w) cm^{-1}. IR (CH_3CN, 293 K) ν_{CO}: 2039 (sh), 2028 (sh), 1940 (m), 1895 (w) cm^{-1}. IR (dmso, 293 K) ν_{CO}: 2038 (sh), 2027 (m), 1937 (s), 1890 (ms) cm^{-1}. ^1H NMR (CD_2Cl_2, 298 K): δ 7.53 (s, 4H, CH_{imid}), 7.04 (s, 8H, CH_{Ar}), 2.46 (s, 12H, CH_3), 1.78 (s, 24H, CH_3). $^{13}C\{^1H\}$ NMR (CD_2Cl_2, 298 K): δ 206.0 (br, CO), 182.5 (C−Ag, $^1J_{C-Ag}$ = 207 and 180 Hz), 139.2, 135.2, 134.5, 129.1, 123.3 (C_{Ar} and CH_{imid}), 20.3, 16.5 (CH_3).

4.7. Synthesis of [Co(CO)$_4${Au(IMes)}] (7). Na[Co(CO)$_4$] (0.190 g, 0.984 mmol) and Au(IMes)Cl (0.530 g, 0.988 mmol) were charged in a Schlenk tube under a nitrogen atmosphere, and THF (15 mL) was added. The mixture was stirred for 30 min at room temperature, and then the solvent was removed under reduced pressure. The crude product was extracted in toluene (15 mL), and a microcrystalline powder of **7** was obtained by slow addition of *n*-pentane (30 mL) (yield 0.49 g, 74%).

$C_{25}H_{24}AuCoN_2O_4$ (672.07): calcd (%): C 44.64, H 3.60, N 4.17. Found: C 44.25, H 3.91, N 3.87. IR (THF, 293 K) ν_{CO}: 2044 (s), 2023 (w), 1967 (s), 1947 (s) cm^{-1}. ^1H NMR (CD_2Cl_2, 298 K): δ 7.19 (s, 2H, CH_{imid}), 7.06 (s, 4H, CH_{Ar}), 2.36 (s, 6H, CH_3), 2.16 (s, 12H, CH_3). $^{13}C\{^1H\}$ NMR (CD_2Cl_2, 298 K): δ 208.0 (br, CO), 185.5 (C−Au), 139.7, 134.8, 134.7, 129.1, 121.9 (C_{Ar} and CH_{imid}), 20.8, 17.4 (CH_3).

4.8. Synthesis of [HIPr]$_2$[Ag$_2${Co(CO)$_4$}$_4$] (11). Complex **2** (0.350 g, 0.524 mmol) and $Co_2(CO)_8$ (0.180 g, 0.527 mmol) were charged in a Schlenk tube under a nitrogen atmosphere, and THF (15 mL) was added. The mixture was heated at refluxing temperature for 300 min, and then the solvent was removed under reduced pressure. The crude product was washed with H_2O (20 mL) and toluene (15 mL) and extracted in CH_2Cl_2 (15 mL). Slow diffusion of *n*-pentane (30 mL) at −20 °C afforded a few crystals of **11**, whereas the majority of product recovered was unreacted **2**. Because of this, yields were not calculated, and **11** was only characterized by SC-XRD.

4.9. Synthesis of [Co$_4$(CO)$_8$(μ-η^7-IMes)] (12). Compound **8** (0.828 g, 0.768 mmol) and $Co_2(CO)_8$ (0.450 g, 1.32 mmol) were charged in a Schlenk tube under a nitrogen atmosphere, and THF (15 mL) was added. The mixture was heated at refluxing temperature for 300 min, and then the solvent was removed under reduced pressure. The crude product was washed with H_2O (20 mL) and extracted with toluene (15 mL). Slow diffusion of *n*-pentane (30 mL) at −20 °C afforded a few crystals of **12**·0.5(toluene), whereas the majority of product recovered was unreacted **8**. Because of this, yields were not calculated, and **11** was only characterized by SC-XRD.

4.10. X-ray Crystallographic Study. Crystal data and collection details for [Co(CO)$_4${Ag(IPr)}] (**2**), [Co(CO)$_4${Au(IPr)}] (**3**), [Ag(IMes)$_2$][Ag{Co(CO)$_4$}$_2$] (**9**), [Cu(IMes)$_2$][Cu{Co(CO)$_4$}$_2$] (**8**), [Cu(IMes)$_2$][Co(CO)$_4$], [HIPr]$_2$[Ag$_2${Co(CO)$_4$}$_4$] (**11**), and [Co$_4$(CO)$_8$(μ-η^7-IMes)]·0.5(toluene) (**12**·0.5(toluene)) are reported in Table S1. The diffraction experiments were carried out on a Bruker APEX II diffractometer equipped with a PHOTON100 detector using Mo Kα radiation. Data were corrected for Lorentz polarization and absorption effects (empirical absorption correction SADABS).[52] Structures were solved by direct methods and refined by full-matrix least-squares based on all data using F^2.[53] Hydrogen atoms were fixed

https://doi.org/10.1021/acs.organomet.1c00363
Organometallics 2021, 40, 2724−2735

at calculated positions and refined by a riding model. All non-hydrogen atoms were refined with anisotropic displacement parameters.

4.11. NMR-Scale Catalytic Test. In a typical test, a capillary containing $BF_3{\cdot}Et_2O$ as reference was inserted into an oven-dried NMR tube, and then the catalyst was added as a solid, followed by 1.00 mL of a solution of AB (45 mg, 1.46 mmol) in freshly distilled THF (10 mL). The catalytic load was 5% mol/mol that in the case of **1** corresponded to 4.5 mg of complex (0.00723 mmol) per 4.5 mg of AB (0.146 mmol). The NMR tube was stored at 298 or 323 K, and the disappearance of AB was monitored by ^{11}B NMR comparing the integral of the resonance of AB vs that of the $BF_3{\cdot}Et_2O$ reference.

4.12. *In Situ* FT-ATR Experiments. *In situ* FT-ATR experiments were carried out using a Bruker Tensor II instrument equipped with a CaF_2 cell. The general procedure for the investigations is the following: First, 3.2 mg of **1** was completely dissolved in anhydrous THF (0.5 mL) in a Schlenk tube under nitrogen atmosphere. In another Schlenk tube, 3.2 mg of AB was completely dissolved in anhydrous THF (0.5 mL) under nitrogen atmosphere. The two solution were mixed closely before transfer to the IR cell under nitrogen atmosphere. The spectra were acquired every 30 s.

4.13. Reactor-Scale Catalytic Test. A solution of AB (64 mg) in THF (10 mL) was mixed with a solution of **1** (64 mg) in THF (10 mL) under nitrogen atmosphere at room temperature in a 200 mL stirred glass reactor. The reactor is equipped with a digital pressure controller and a rubber septum for syringe sampling. During reaction, the reactor head was sampled every 5 min and analyzed in a gas chromatograph equipped with a TCD detector. The pressure of the system was monitored and used to determine the amount of H_2 produced.

4.14. Computational Details. All density functional theory (DFT) calculations were carried out using the Gaussian 16 package[54] and the B3LYP functional.[55−57] Geometry optimizations and frequencies computations were performed using the 6-31G(d,p) basis set for all atoms,[58] except for transition metals, for which the LANL2DZ basis set with pseudopotentials[59] was used. The nature of each optimized geometry was confirmed by analytical frequencies analysis carried out at the same level of theory, along with natural bond analysis,[47] as implemented in Gaussian 16. Computed IR frequencies reported were rescaled using a 0.961 scaling factor.[60] Refined energies for thermodynamics were obtained by single-point calculations computed on optimized geometries, using a larger basis set (i.e., 6-311+G(2d,2p) for all atoms but transition metals), adding Gibbs free energy corrections at room temperature and Grimme-D3 corrections[61] for dispersion, and including the conduction-like polarizable continuum model (C-PCM) for solvation effects.[62,63]

■ ASSOCIATED CONTENT

Supporting Information

The Supporting Information is available free of charge at https://pubs.acs.org/doi/10.1021/acs.organomet.1c00363.

Experimental and simulated IR spectra. NMR spectra. X-ray crystallographic data and details (PDF)

Optimized coordinates in XYZ format (XYZ)

Accession Codes

CCDC 2089181−2089187 contain the supplementary crystallographic data for this paper. These data can be obtained free of charge via www.ccdc.cam.ac.uk/data_request/cif, or by emailing data_request@ccdc.cam.ac.uk, or by contacting The Cambridge Crystallographic Data Centre, 12 Union Road, Cambridge CB2 1EZ, UK; fax: +44 1223 336033.

■ AUTHOR INFORMATION

Corresponding Author

Stefano Zacchini − *Dipartimento di Chimica Industriale "Toso Montanari", Università di Bologna, I-40136 Bologna, Italy;* orcid.org/0000-0003-0739-0518; Phone: +39 051 2093711; Email: stefano.zacchini@unibo.it; https://www.unibo.it/sitoweb/stefano.zacchini/en

Authors

Cristiana Cesari − *Dipartimento di Chimica Industriale "Toso Montanari", Università di Bologna, I-40136 Bologna, Italy;* orcid.org/0000-0003-2595-2078

Beatrice Berti − *Dipartimento di Chimica Industriale "Toso Montanari", Università di Bologna, I-40136 Bologna, Italy*

Francesco Calcagno − *Dipartimento di Chimica Industriale "Toso Montanari", Università di Bologna, I-40136 Bologna, Italy;* orcid.org/0000-0002-0986-4425

Carlo Lucarelli − *Dipartimento di Scienza e Alta Tecnologia, Università dell'Insubria, I-22100 Como, Italy;* orcid.org/0000-0002-5098-0575

Marco Garavelli − *Dipartimento di Chimica Industriale "Toso Montanari", Università di Bologna, I-40136 Bologna, Italy;* orcid.org/0000-0002-0796-289X

Rita Mazzoni − *Dipartimento di Chimica Industriale "Toso Montanari", Università di Bologna, I-40136 Bologna, Italy;* orcid.org/0000-0002-8926-9203

Ivan Rivalta − *Dipartimento di Chimica Industriale "Toso Montanari", Università di Bologna, I-40136 Bologna, Italy; Université de Lyon, École Normale Supérieure de Lyon, CNRS UMR 5182, Laboratoire de Chimie, F69364 Lyon, France;* orcid.org/0000-0002-1208-602X

Complete contact information is available at: https://pubs.acs.org/10.1021/acs.organomet.1c00363

Funding

The financial support of the University of Bologna is gratefully acknowledged.

Notes

The authors declare no competing financial interest.

■ ACKNOWLEDGMENTS

I.R. gratefully acknowledges the use of HPC resources of the "Pôle Scientifique de Modélisation Numérique" (PSMN) of the ENS-Lyon, France

■ REFERENCES

(1) Banerjee, S.; Karunananda, M. K.; Bagherzadeh, S.; Jayarathne, U.; Parmelee, S. R.; Waldhart, G. W.; Mankad, N. P. Synthesis and Characterization of Heterobimetallic Complexes with Direct Cu-M Bonds (M = Cr, Mn, Co, Mo, Ru, W) Supported by *N*-Heterocyclic Carbene Ligands: A Toolkit for Catalytic Reaction Discovery. *Inorg. Chem.* **2014**, *53*, 11307−11315.

(2) Mankad, N. P. Selectivity Effects in Bimetallic Catalysis. *Chem. - Eur. J.* **2016**, *22*, 5822−5829.

(3) (a) Pye, D. R.; Mankad, N. P. Bimetallic catalysis for C-C and C-X coupling reactions. *Chem. Sci.* **2017**, *8*, 1705−1718. (b) Yu, H.-C.; Mankad, N. P. Catalytic Reactions by Heterobimetallic Carbonyl Complexes with Polar Metal-Metal Interactions. *Synthesis* **2021**, *53*, 1409−1422.

(4) Mankad, N. P. Diverse bimetallic mechanisms emerging from transition metal Lewis acid/base pairs: development of co-catalysis with metal carbenes and metal carbonyl anions. *Chem. Commun.* **2018**, *54*, 1291−1302.

(5) Lakliang, Y.; Mankad, N. P. Heterometallic Cu_2Fe and Zn_2Fe_2 Complexes Derived from $[Fe(CO)_4]^{2-}$ and Cu/Fe Bifunctional N_2O Activation Reactivity. *Organometallics* **2020**, *39*, 2043−2046.

(6) Bauer, J.; Braunschweig, H.; Dewhurst, R. D. Metal-Only Lewis Pairs with Transition Metal Lewis Bases. *Chem. Rev.* **2012**, *112*, 4329−4346.
(7) Ma, M.; Sidiropoulos, A.; Ralte, L.; Stasch, A.; Jones, C. Metal-only Lewis pairs featuring unsupported PtMM (M = Zn or Cd) dative bonds. *Chem. Commun.* **2013**, *49*, 48−50.
(8) Campos, J. Dihydrogen and Acetylene Activation by a Gold(I)/Platinum(0) Transition Metal Only Frustrated Lewis Pair. *J. Am. Chem. Soc.* **2017**, *139*, 2944−2947.
(9) Berti, B.; Bortoluzzi, M.; Cesari, C.; Femoni, C.; Iapalucci, M. C.; Mazzoni, R.; Zacchini, S. A Comparative Experimental and Computational Study of Heterometallic Fe-M (M = Cu, Ag, Au) Carbonyl Clusters Containing N-Heterocyclic Carbene Ligands. *Eur. J. Inorg. Chem.* **2020**, *2020*, 2191−2202.
(10) Berti, B.; Bortoluzzi, M.; Cesari, C.; Femoni, C.; Iapalucci, M. C.; Mazzoni, R.; Vacca, F.; Zacchini, S. Thermal Growth of Au-Fe Heterometallic Carbonyl Clusters Containing N-Heterocyclic Carbene and Phosphine Ligands. *Inorg. Chem.* **2020**, *59*, 2228−2240.
(11) Berti, B.; Bortoluzzi, M.; Cesari, C.; Femoni, C.; Iapalucci, M. C.; Mazzoni, R.; Vacca, F.; Zacchini, S. Synthesis and Characterization of Heterobimetallic Carbonyl Clusters with Direct Au-Fe and Au&Au Interactions Supported by *N*-Heterocyclic Carbene and Phosphine Ligands. *Eur. J. Inorg. Chem.* **2019**, *2019*, 3084−3093.
(12) Berti, B.; Bortoluzzi, M.; Cesari, C.; Femoni, C.; Iapalucci, M. C.; Mazzoni, R.; Vacca, F.; Zacchini, S. Polymerization Isomerism in $[\{MFe(CO)_4\}_n]^{n-}$ (M = Cu, Ag, Au; n = 3, 4) Molecular Clusters Supported by Metallophilic Interactions. *Inorg. Chem.* **2019**, *58*, 2911−2915.
(13) Bortoluzzi, M.; Cesari, C.; Ciabatti, I.; Femoni, C.; Hayatifar, M.; Iapalucci, M. C.; Mazzoni, R.; Zacchini, S. Bimetallic Fe-Au Carbonyl Clusters Derived from Collman's Reagent: Synthesis, Structure and DFT Analysis of $Fe(CO)_4(AuNHC)_2$ and $[Au_3Fe_2(CO)_8(NHC)_2]^-$. *J. Cluster Sci.* **2017**, *28*, 703−723.
(14) Nugent, J. W.; García-Melchor, M.; Fout, A. R. Cobalt-Catalyzed Ammonia Borane Dehydrogenation: Mechanistic Insight and Isolation of a Cobalt Hydride-Amidoborane Complex. *Organometallics* **2020**, *39*, 2917−2927.
(15) Li, H.; Yang, Q.; Chen, X.; Shore, S. G. Ammonia borane, past as prolog. *J. Organomet. Chem.* **2014**, *751*, 60−66.
(16) Keaton, R. J.; Blacquiere, J. M.; Baker, R. T. Base Metal Catalyzed Dehydrogenation of Ammonia-Borane for Chemical Hydrogen Storage. *J. Am. Chem. Soc.* **2007**, *129*, 1844−1845.
(17) Kumar, R.; Karkamkar, A.; Bowden, M.; Autrey, T. Solid-state hydrogen rich boron-nitrogen compounds for energy storage. *Chem. Soc. Rev.* **2019**, *48*, 5350−5380.
(18) Mal, S. S.; Stephens, F. H.; Baker, R. T. Transition metal catalysed dehydrogenation of amine-borane fuel blends. *Chem. Commun.* **2011**, *47*, 2922−2924.
(19) Hamilton, C. W.; Baker, R. T.; Staubitz, A.; Manners, I. B-N compounds for chemical hydrogen storage. *Chem. Soc. Rev.* **2009**, *38*, 279−293.
(20) Conley, B. L.; Guess, D.; Williams, T. J. A Robust, Air-Stable, Reusable Ruthenium Catalyst for Dehydrogenation of Ammonia Borane. *J. Am. Chem. Soc.* **2011**, *133*, 14212−14215.
(21) Lu, Z.; Conley, B. L.; Williams, T. J. A Three-Stage Mechanistic Model for Ammonia-Borane Dehydrogenation by Shvo's Catalyst. *Organometallics* **2012**, *31*, 6705−6714.
(22) Zhang, X.; Kam, L.; Williams, T. J. Dehydrogenation of ammonia borane through the third equivalent of hydrogen. *Dalton Trans.* **2016**, *45*, 7672−7677.
(23) Zhang, X.; Kam, L.; Trerise, R.; Williams, T. J. Ruthenium-Catalyzed Ammonia Borane Dehydrogenation: Mechanism and Utility. *Acc. Chem. Res.* **2017**, *50*, 86−95.
(24) Baker, R. T.; Gordon, J. C.; Hamilton, C. W.; Henson, N. J.; Lin, P.-H.; Maguire, S.; Murugesu, M.; Scott, B. L.; Smythe, N. Iron Complex-Catalyzed Ammonia-Borane Dehydrogenation. A Potential Route toward B-N-Containing Polymer Motifs Using Earth-Abundant Metal Catalysts. *J. Am. Chem. Soc.* **2012**, *134*, 5598−5609.
(25) Rossin, A.; Peruzzini, M. Ammonia-Borane and Amine-Borane Dehydrogenation Mediated by Complex Metal Hydrides. *Chem. Rev.* **2016**, *116*, 8848−8872.
(26) Blundell, T. L.; Powell, H. M. Stereochemistry of cobalt complexes with heteronuclear metal-metal bonds: the crystal and molecular structure of tetracarbonyl(triphenylphosphineaurio)cobalt, and of tetracarbonyl{[bis-(*o*-dimethylarsinophenyl)methylarsine]-argentio}cobalt. *J. Chem. Soc. A* **1971**, *0*, 1685−1690.
(27) Braunstein, P.; Rosé, J.; Dedieu, A.; Dusausoy, Y.; Mangeot, J.-P.; Tiripicchio, A.; Tiripicchio-Camellini, M. Syntheses, structures, and bonding of heteropentametallic clusters $[MCo_3(CO)_{12}\{\{_3\text{-}M'(EPh_3)\}\}]$ (M = Fe or Ru; M′ = Cu or Au; E = P or As): X-ray crystal structures of $[RuCo_3(CO)_{12}\{\{_3\text{-}M'(PPh_3)\}\}]$ (M′ = Cu or Au). *J. Chem. Soc., Dalton Trans.* **1986**, 225−234.
(28) Cotton, F. A.; Daniels, L. M.; Murillo, C. A.; Zhou, H. C. The Effect of Divergent-Bite Ligands on Metal-Metal Bond Distances in Some Paddlewheel Complexes. *Inorg. Chim. Acta* **2000**, *300*−*302*, 319−327.
(29) Pauling, L. Atomic Radii and Interatomic Distances in Metals. *J. Am. Chem. Soc.* **1947**, *69*, 542−553.
(30) Cesari, C.; Berti, B.; Calcagno, F.; Femoni, C.; Garavelli, M.; Iapalucci, M. C.; Rivalta, I.; Zacchini, S. Polymerization Isomerism in Co−M (M = Cu, Ag, Au) Carbonyl Clusters: Synthesis, Structures and Computational Investigation. *Molecules* **2021**, *26*, 1529.
(31) Darensbourg, D. J.; Chao, C. S.; Reibenspies, J. H.; Bischoff, C. J. Crystal structure and reactivity of bis[bis(1,2-dimethylphosphino)-ethane]copper(2+) bis(tetracarbonylcobalt)cuprate(2-): staggered and eclipsed conformations of $[(CO)_4CoCuCo(CO)_4]^-$ anions. *Inorg. Chem.* **1990**, *29*, 2153−2157.
(32) Fuchs, R.; Klüfers, P. Heteronukleare Komplex verbindungen mit Metall-Metall Bindungen, V. Umsetzungen mit $[(NH_3)_2CuCo(CO)_4]$: Synthese und Struktur von $[(PPh_3)_2CuCo(CO)_4]$, $[Cu\{P(OMe)_3\}_4][Cu\{Co(CO)_4\}_2]$ und $(Ph_3P)_2N[Cu\{Co(CO)_4\}_2]$. *Z. Naturforsch., B: J. Chem. Sci.* **1991**, *46*, 507−518.
(33) Usón, R.; Laguna, A.; Laguna, M.; Jones, P. G.; Sheldrick, G. M. Novel compounds with gold-transition-metal bonds; crystal and molecular structure of bis(triphenylphosphine)iminium bis-(tetracarbonylcobaltio)aurate(I). *J. Chem. Soc., Dalton Trans.* **1981**, 366−370.
(34) Klüfers, P. Die Kristallstruktur von $AgCo(CO)_4$. *Z. Kristallogr. - Cryst. Mater.* **1984**, *166*, 143−151.
(35) Schmidbaur, H.; Schier, A. Argentophilic Interactions. *Angew. Chem., Int. Ed.* **2015**, *54*, 746−784.
(36) (a) Hong, S. H.; Day, M. W.; Grubbs, R. H. Decomposition of a Key Intermediate in Ruthenium-Catalyzed Olefin Metathesis Reactions. *J. Am. Chem. Soc.* **2004**, *126*, 7414−7415. (b) Meier, S. C.; Holz, A.; Kulenkampff, J.; Schmidt, A.; Kratzert, D.; Himmel, D.; Schmitz, D.; Scheidt, E.-W.; Scherer, W.; Bülow, C.; Timm, M.; Lindblad, R.; Akin, S. T.; Zamudio-Bayer, V.; von Issendorff, B.; Duncan, M. A.; Lau, T. J.; Krossing, I. Access to the Bis-benzene Cobalt(I) Sandwich Cation and its Derivatives: Synthons for a "Naked" Cobalt(I) Source? *Angew. Chem., Int. Ed.* **2018**, *57*, 9310−9314.
(37) (a) Rubio-Pérez, L.; Iglesias, M.; Munárriz, J.; Polo, V.; Sanz Miguel, P. J.; Pérez-Torrente, J. J.; Oro, L. A. A bimetallic iridium(II) catalyst: $[\{Ir(IDipp)(H)\}_2][BF_4]_2$ (IDipp = 1,3-bis(2,6-diisopropylphenylimidazol-2-ylidene)). *Chem. Commun.* **2015**, *51*, 9860−9863. (b) Hashimoto, T.; Hoshino, R.; Hatanaka, T.; Ohki, Y.; Tatsumi, K. Dinuclear Iron(0) Complexes of N-Heterocyclic Carbenes. *Organometallics* **2014**, *33*, 921−929.
(38) (a) Tang, C. Y.; Lednik, J.; Vidovic, D.; Thompson, A. L.; Aldridge, S. Responses to unsaturation in iridium mono(*N*-heterocyclic carbene) complexes: synthesis and oligomerization of $[LIr(H)_2Cl]$ and $[LIr(H)_2]^+$. *Chem. Commun.* **2011**, *47*, 2523−2525. (b) Lee, C. H.; Laitar, D. S.; Mueller, P.; Sadighi, J. P. Generation of a Doubly Bridging CO_2 Ligand and Deoxygenation of CO_2 by an (NHC)Ni(0) Complex. *J. Am. Chem. Soc.* **2007**, *129*, 13802−13803.
(39) Kolychev, E. L.; Kronig, S.; Brandhorst, K.; Freytag, M.; Jones, P. G.; Tamm, M. Iridium(I) Complexes with Anionic N-Heterocyclic

https://doi.org/10.1021/acs.organomet.1c00363
Organometallics 2021, 40, 2724−2735

Carbene Ligands as Catalysts for the Hydrogenation of Alkenes in Nonpolar Media. *J. Am. Chem. Soc.* **2013**, *135*, 12448−12459.
(40) Cabeza, J. A.; del Rio, I.; Fernandez-Colinas, J. M.; Perez-Carreno, E.; Sanchez-Vega, M. G.; Vazquez-Garcia, D. Reactivity of $[Ru_4((-H)_4(CO)_{12}]$ with N-Heterocyclic Carbenes. *Organometallics* **2009**, *28*, 1832−1837.
(41) Chini, P.; Albano, V. Synthesis and properties of pentadecacarbonyl-hexacobaltate dianion derivatives. *J. Organomet. Chem.* **1968**, *15*, 433−440.
(42) Zhang, J.; Zhao, Y.; Akins, D. L.; Lee, J. W. Thermal Decomposition and Spectroscopic Studies of Preheated Ammonia Borane. *J. Phys. Chem. C* **2010**, *114*, 19529−19534.
(43) Al-Kukhun, A.; Hwang, H. T.; Varma, A. Mechanistic studies of ammonia borane dehydrogenation. *Int. J. Hydrogen Energy* **2013**, *38*, 169−179.
(44) Kantürk Figen, A.; Piskin, M. B.; Coskuner, B.; İmamoğlu, V. Synthesis, structural characterization, and hydrolysis of Ammonia Borane (NH_3BH_3) as a hydrogen storage carrier. *Int. J. Hydr. En.* **2013**, *38*, 16215−16228.
(45) Paolone, A.; Teocoli, F.; Sanna, S.; Palumbo, O.; Autrey, T. Temperature Dependence of the Infrared Spectrum of Ammonia Borane: Librations, Rotations, and Molecular Vibrations. *J. Phys. Chem. C* **2013**, *117*, 729−734.
(46) Wiberg, K. B. Application of the Pople-Santry-Segal CNDO Method to the Cyclopropylcarbinyl and Cyclobutyl Cation and to Bicyclobutane. *Tetrahedron* **1968**, *24*, 1083−1096.
(47) Reed, A. E.; Weinstock, R. B.; Weinhold, F. Natural-population analysis. *J. Chem. Phys.* **1985**, *83*, 735−746.
(48) Parmelee, S. R.; Mankad, N. P. A data-intensive re-evaluation of semibridging carbonyl ligands. *Dalton Trans.* **2015**, *44*, 17007−17014.
(49) Sun, C.; Teo, B. K.; Deng, C.; Lin, J.; Luo, G.-G.; Tung, C.-H.; Sun, D. Hydrido-coinage-metal clusters: Rational design, synthetic protocols and structural characteristics. *Coord. Chem. Rev.* **2021**, *427*, 213576.
(50) Edgell, W. F.; Lyford, J. The Preparation of Sodium Cobalt Tetracarbonyl. *Inorg. Chem.* **1970**, *9*, 1932−1933.
(51) (a) Collado, A.; Gómez-Suárez, A.; Martin, A. R.; Slawin, A. M. Z.; Nolan, S. P. Straightforward synthesis of [Au(NHC)X] (NHC = *N*-heterocyclic carbene, X = Cl, Br, I) complexes. *Chem. Commun.* **2013**, *49*, 5541−5543. (b) de Frémont, P.; Scott, N. M.; Stevens, E. D.; Ramnial, T.; Lightbody, O. C.; Macdonald, C. L. B.; Clyburne, J. A. C.; Abernethy, C. D.; Nolan, S. P. Synthesis of Well-Defined *N*-Heterocyclic Carbene Silver(I) Complexes. *Organometallics* **2005**, *24*, 6301−6309.
(52) Sheldrick, G. M. *SADABS-2008/1 - Bruker AXS Area Detector Scaling and Absorption Correction*; Bruker AXS: Madison, WI, 2008.
(53) Sheldrick, G. M. Crystal Structure Refinement with SHELXL. *Acta Crystallogr., Sect. C: Struct. Chem.* **2015**, *71*, 3−8.
(54) Frisch, M. J.; Trucks, G. W.; Schlegel, H. B.; Scuseria, G. E.; Robb, M. A.; Cheeseman, J. R.; Scalmani, G.; Barone, V.; Petersson, G. A.; Nakatsuji, H.; Li, X.; Caricato, M.; Marenich, A. V.; Bloino, J.; Janesko, B. G.; Gomperts, R.; Mennucci, B.; Hratchian, H. P.; Ortiz, J. V.; Izmaylov, A. F.; Sonnenberg, J. L.; Williams-Young, D.; Ding, F.; Lipparini, F.; Egidi, F.; Goings, J.; Peng, B.; Petrone, A.; Henderson, T.; Ranasinghe, D.; Zakrzewski, V. G.; Gao, J.; Rega, N.; Zheng, G.; Liang, W.; Hada, M.; Ehara, M.; Toyota, K.; Fukuda, R.; Hasegawa, J.; Ishida, M.; Nakajima, T.; Honda, Y.; Kitao, O.; Nakai, H.; Vreven, T.; Throssell, K.; Montgomery, J. A., Jr.; Peralta, J. E.; Ogliaro, F.; Bearpark, M.; Heyd, J. J.; Brothers, E. N.; Kudin, K. N.; Staroverov, V. N.; Kobayashi, R.; Normand, J.; Raghavachari, K.; Rendell, A.; Burant, J. C.; Iyengar, S. S.; Tomasi, J.; Cossi, M.; Millam, J. M.; Klene, M.; Adamo, C.; Cammi, R.; Ochterski, J. W.; Martin, R. L.; Morokuma, K.; Farkas, O.; Foresman, J. B.; Fox, D. J. *Gaussian 16*, revision C.01; Gaussian, Inc.: Wallingford CT, 2016.
(55) Becke, A. D. Density-Functional Thermochemistry. III. The Role of Exact Exchange. *J. Chem. Phys.* **1993**, *98*, 5648−5652.
(56) Lee, C.; Yang, W.; Parr, R. G. Development of the Colle-Salvetti Correlation-Energy Formula into a Functional of the Electron Density. *Phys. Rev. B: Condens. Matter Mater. Phys.* **1988**, *37*, 785−789.
(57) Dolg, M.; Wedig, U.; Stoll, H.; Preuss, H. Energy-Adjusted ab initio Pseudopotentials for the First Row Transition Elements. *J. Chem. Phys.* **1987**, *86*, 866−872.
(58) Francl, M. M.; Pietro, W. J.; Hehre, W. J.; Binkley, J. S.; De Frees, D. J.; Pople, J. A.; Gordon, M. S. Self-Consistent Molecular Orbital Methods. 23. A polarization-type basis set for 2nd-row elements. *J. Chem. Phys.* **1982**, *77*, 3654−3665.
(59) Hay, P. J.; Wadt, W. R. Ab initio effective core potentials for molecular calculations-potentials for K to Au including the outermost core orbitals. *J. Chem. Phys.* **1985**, *82*, 299−310.
(60) Russell, D. J., III, Ed. *NIST Computational Chemistry Comparison and Benchmark Database; NIST Standard Reference Database Number 101*; Release 21 August 2020; The National Institute of Standards and Technology (NIST): Gaithersburg, MD, 2020. http://cccbdb.nist.gov/.
(61) Grimme, S.; Antony, J.; Ehrlich, S.; Krieg, H. A consistent and accurate ab initio parameterization of density functional dispersion correction (DFT-D) for the 94 elements H-Pu. *J. Chem. Phys.* **2010**, *132*, 154104.
(62) Barone, V.; Cossi, M. Quantum calculation of molecular energies and energy gradients in solution by a conductor solvent model. *J. Phys. Chem. A* **1998**, *102*, 1995−2001.
(63) Cossi, M.; Rega, N.; Scalmani, G.; Barone, V. Energies, structures, and electronic properties of molecules in solution with the C-PCM solvation model. *J. Comput. Chem.* **2003**, *24*, 669−681.

https://doi.org/10.1021/acs.organomet.1c00363
Organometallics 2021, 40, 2724−2735